NEOPLASIA
www.neoplasia.com

Volume 13 Number 8 August 2011 pp. 676–684 676

Enhanced Expression of EHMT2 Is Involved in the Proliferation of Cancer Cells through Negative Regulation of SIAH1[1,2]

Hyun-Soo Cho*, John D. Kelly†,‡, Shinya Hayami*, Gouji Toyokawa*, Masahi Takawa*, Masanori Yoshimatsu*, Tatsuhiko Tsunoda§, Helen I. Field¶, David E. Neal†, Bruce A.J. Ponder†, Yusuke Nakamura* and Ryuji Hamamoto*,†

*Laboratory of Molecular Medicine, Human Genome Center, Institute of Medical Science, The University of Tokyo, Tokyo, Japan; †Department of Oncology, Cancer Research UK Cambridge Research Institute, University of Cambridge, Cambridge, UK; ‡Division of Surgery & Interventional Science, UCL Medical School, University College London, London, UK; §Laboratory for Medical Informatics, RIKEN, Kanagawa, Japan; ¶Department of Genetics, University of Cambridge, Cambridge, UK

Abstract

EHMT2 is a histone lysine methyltransferase localized in euchromatin regions and acting as a corepressor for specific transcription factors. Although the role of EHMT2 in transcriptional regulation has been well documented, the pathologic consequences of its dysfunction in human disease have not been well understood. Here, we describe important roles of EHMT2 in human carcinogenesis. Expression levels of *EHMT2* are significantly elevated in human bladder carcinomas compared with nonneoplastic bladder tissues ($P < .0001$) in real-time polymerase chain reaction analysis. Complementary DNA microarray analysis also revealed its overexpression in various types of cancer. The reduction of EHMT2 expression by small interfering RNAs resulted in the suppression of the growth of cancer cells and possibly caused apoptotic cell death in cancer cells. Importantly, we show that EHMT2 can suppress transcription of the *SIAH1* gene by binding to its promoter region (−293 to +51) and by methylating lysine 9 of histone H3. Furthermore, an EHMT2-specific inhibitor, BIX-01294, significantly suppressed the growth of cancer cells. Our results suggest that dysregulation of EHMT2 plays an important role in the growth regulation of cancer cells, and further functional studies may affirm the importance of EHMT2 as a promising therapeutic target for various types of cancer.

Neoplasia (2011) 13, 676–684

Introduction

Histone methylation plays dynamic and crucial roles in regulating chromatin structure. Precise coordination and organization of open and closed chromatin regions control normal cellular processes such as DNA replication, repair, recombination, and transcription. Histone lysine methylation is considered to regulate the transcription positively or negatively depending on the methylation sites and the methylation status [1]. For instance, methylation of histone H3 at lysine 9 (H3K9) has served as the prototype for studying the regulation of histone function by lysine methylation. Dimethylation or trimethylation of H3K9 creates a binding site for chromodomain-containing proteins of the

Address all correspondence to: Ryuji Hamamoto, PhD, Laboratory of Molecular Medicine, Human Genome Center, Institute of Medical Science, The University of Tokyo, 4-6-1 Shirokanedai, Minato-ku, Tokyo 108-8639, Japan. E-mail: ryuji@ims.u-tokyo.ac.jp

[1]Our biorepository is supported by funding from the National Institute for Health Research and the Cambridge Biomedical Research Centre. This work was supported by a Grant-in-Aid for Young Scientists (A) (22681030) from the Japan Society for the Promotion of Science.

[2]This article refers to supplementary materials, which are designated by Tables W1 to W5 and Figures W1 to W3 and are available online at www.neoplasia.com.

Received 9 April 2011; Revised 29 May 2011; Accepted 31 May 2011

DOI 10.1593/neo.11512

heterochromatin protein 1 family [2,3], which is speculated to lead to gene repression through changes in higher-order chromatin structure. Methylation-dependent heterochromatin protein 1 recruitment can be antagonized by adjacent H3 serine 10 phosphorylation. Thus, histones are subject to a system of combinatorially acting posttranslational modifications, referred to as the "histone code" [4–6]. Despite a large body of information for the prominent role of histone methylation in transcriptional regulation, their physiological function and their involvement in human disease are still not well understood. We previously reported that the histone methyltransferase SMYD3 stimulates cell proliferation through its methyltransferase activity and plays a crucial role in human carcinogenesis [7,8], and several groups also showed that deregulation of histone methyltransferases could be involved in human carcinogenesis [9,10]. To find other methyltransferases involved in human carcinogenesis, we examined expression profiles for a number of histone methyltransferases using clinical tissues and found transactivation of EHMT2 in nine types of tumors, including bladder and lung cancers.

EHMT2, also known as G9a, is mainly responsible for monomethylation and dimethylation of H3K9 in euchromatin [11]. EHMT2 is essential for early embryonic development and is involved in the transcriptional silencing of developmentally regulated genes. Knockout of EHMT2 causes embryonic lethality in mice, indicating a major role for epigenetic repression in early mammalian development [12]. Previous studies found that EHMT2 functions as a corepressor, targeted to specific genes by associating with various transcriptional repressors and corepressors: CDP/Cut, Blimp-1/PRDI-BF1, and REST/NRSF [13–15]. Meanwhile, EHMT2 also seems to function as a coactivator for nuclear receptors, collaborating synergistically with CARM1 and other nuclear receptor coactivators [16]. In addition, the complex of EHMT2 and DNMT1 led to enhanced DNA and histone methylation of *in vitro* assembled chromatin substrates, indicating that direct cooperation between EHMT2 and DNMT1 provides a mechanism of H3K9 methylation and coordinated DNA during cell division [17].

SIAH (seven in absentia homolog) proteins are members of the RING-finger-containing E3 ubiquitin ligases. They are homologs of the *Drosophila* seven in absentia (Sina) protein [18,19]. It has been suggested that the SIAH1 protein plays a key role in biologic processes such as the cell cycle, cell apoptosis, and oncogenesis [20–22]. Here, we demonstrate the possible involvement of EHMT2 in human carcinogenesis and direct transcriptional regulation of SIAH1 by EHMT2. These results imply that EHMT2 is a candidate therapeutic target for various types of cancer.

Materials and Methods

Cell Culture

Cancer cell lines used in this study were as follows: lung adenocarcinoma = LC319 and A549; lung squamous cell carcinoma = H2170, RERF-LC-AI; small cell lung cancer = SBC-5; bladder cancer = 5637, 253J, 253JBV, EJ28, HT1197, HT1376, J82, RT4, SCaBER, SW780, T24, and UMUC3. The normal human lung fibroblast HFL-1 and the normal human colon fibroblast CCD-18Co were used as normal control cells. All cell lines were grown in monolayers in appropriate media: Dulbecco modified Eagle medium for EJ28, RERF-LC-AI, and 293T cells; Eagle minimal essential medium for CCD-18Co, 253J, IMR90, WI38, 253J-BV, HT1197, HT1376, J82, SCaBER, UMUC3, and SBC5 cells; F-12K medium for HFL-1 cells; Leibovitz L-15 for SW780 cells; McCoy 5A medium for RT4 and T24 cells; RPMI-1640 medium for 5637, A549, H2170, and LC319 cells supplemented with 10% fetal bovine serum and 1% antibiotic/antimycotic solution (Sigma-Aldrich, St Louis, MO). All cells were maintained at 37°C in humid air with 5% CO_2 condition (CCD-18Co, HFL-1, IMR90, WI38, H2170, 5637, 253J, 253J-BV, EJ28, HT1197, HT1376, J82, RT4, SCaBER, T24, UMUC3, A549, LC319, RERF-LC-AI, SBC5, and 293T) or without CO_2 (SW780). Cells were transfected with FuGENE6 (Roche Applied Science, Basel, Switzerland) according to the manufacturer's protocols.

Immunohistochemical Staining and Tissue Microarray

Immunohistochemical analysis was performed using a specific polyclonal rabbit-EHMT2 antibody as described previously [23,24]. For clinical bladder tissue microarray, VECTASTAIN ABC Kit (Vector Laboratories, Burlingame, CA) was applied. Briefly, endogenous peroxidase activity of xylene-deparaffinized and dehydrated sections was inhibited by treatment with 0.3% H_2O_2/methanol. Nonspecific binding was blocked by incubating sections with 3% bovine serum albumin in a humidified chamber for 30 minutes at ambient temperature, then a 1:1000 dilution of rabbit polyclonal anti-EHMT2 antibody (NB100-40825; Novus Biologicals, Littleton, CO) overnight at 4°C. Sections were washed twice with phosphate-buffered saline, incubated with 1 μg/μl goat antirabbit biotinylated IgG in phosphate-buffered saline containing 1% bovine serum albumin for 30 minutes at ambient temperature and then incubated with ABC reagent for 30 minutes. Immunostaining was visualized using 3,3′-diaminobenzidine. Slides were dehydrated through graded alcohol to xylene washing and mounted on coverslips. Hematoxylin was used for nuclear counterstaining. For clinical lung cancer tissue microarray, EnVision+ kit/horseradish peroxidase (Dako, Glostrup, Denmark) was applied. Briefly, slides of paraffin-embedded lung tumor specimens were processed under high pressure (125°C for 30 seconds) in an antigen-retrieval solution, high pH 9 (S2367; Dako Cytomation, Carpinteria, CA), treated with peroxidase blocking reagent, and then treated with a protein blocking reagent (K130, X0909; Dako Cytomation). Tissue sections were incubated with a rabbit anti-EHMT2 polyclonal antibody followed by HRP-conjugated secondary antibody (Dako Cytomation). The antigen was visualized with a substrate chromogen (Dako liquid DAB chromogen; Dako Cytomation). Finally, tissue specimens were stained with Mayer hematoxylin (Muto Pure Chemicals Ltd, Tokyo, Japan) for 20 seconds to discriminate the nucleus from the cytoplasm.

Quantitative Real-time Polymerase Chain Reaction

As described previously, we obtained 118 bladder cancer tissues and 26 normal bladder tissues from Addenbrooke's Hospital, Cambridge. For quantitative reverse transcription–polymerase chain reactions (RT-PCRs), specific primers for all human *GAPDH* (housekeeping gene), *SDH* (housekeeping gene), and *EHMT2* were designed (primer sequences in Table W5). PCRs were performed using the ABI Prism 7700 Sequence Detection System (Applied Biosystems, Warrington, United Kingdom) following the manufacturer's protocol. Moreover, 50% SYBR Green Universal PCR MasterMix without UNG (Applied Biosystems), 50 nM each of the forward and reverse primers, and 2 μl of reverse-transcribed complementary DNA (cDNA) were applied. Amplification conditions were 5 minutes at 95°C and then 45 cycles each consisting of 10 seconds at 95°C, 1 minute at 55°C, and 10 seconds at 72°C. Then, reactions were heated for 15 seconds at 95°C, 1 minute at 65°C to draw the melting curve, and cooled to 50°C for 10 seconds. Reaction conditions for target gene amplification were as

described previously, and the equivalent of 5 ng of reverse-transcribed RNA was used in each reaction. Messenger RNA (mRNA) levels were normalized to *GAPDH* and *SDH* expressions.

Small Interfering RNA Transfection

Small interfering RNA (siRNA) oligonucleotide duplexes were purchased from SIGMA Genosys (St Louis, MO) for targeting the human *EHMT2* and *SIAH1* transcripts. siEGFP, siFFLuc, and siNegative Control (siNC) were used as controls. siRNA sequences are described in Table W2. siRNA duplexes (final concentration, 100 nM) were transfected in lung cancer cell lines with Lipofectamine 2000 (Invitrogen, Carlsbad, CA) for 72 hours, and cell viability was examined using Cell Counting Kit 8 (DOJINDO, Kumamoto, Japan).

Flow Cytometry Assays for Cell Cycle Analysis

We collected the cells after trypsin treatment, washed them twice with 1000 μl of assay buffer, and centrifuged for 5 minutes at 5000 rpm. Cells were resuspended in 200 μl of assay buffer. One thousand microliters of fixative buffer was added, and the samples were incubated at room temperature for 1 hour. Finally, we added the propidium iodide reagent and analyzed the cell cycle profiles by flow cytometry (LSR II; BD Biosciences, Franklin Lakes, NJ). The proportion of each cell division was calculated and analyzed using Student's *t* test for significance.

Chromatin Immunoprecipitation Assay

Chromatin immunoprecipitation (ChIP) assays were performed using ChIP Assay Kit (Millipore, Billerica, MA) according to the manufacturer's protocol. Briefly, the fragment of EHMT2 and chromatin complexes was immunoprecipitated with anti-FLAG antibody 48 hours after transfection with pCAGGS-n3FC (Mock) and pCAGGS-n3FC-EHMT2 (3×FLAG-EHMT2) vectors. After the bound DNA fragments to EHMT2 were eluted, the amount was subjected to quantitative real-time PCRs. Primer sequences are shown in Table W5.

Microarray Hybridization and Statistical Analysis for the Clarification of Downstream Genes

Microarray analysis to identify downstream genes were done described previously [25–27]. Briefly, purified total RNA was labeled and hybridized onto Affymetrix GeneChip U133 Plus 2.0 oligonucleotide arrays (Affymetrix, Santa Clara, CA) according to the manufacturer's instructions. We performed a pathway analysis using the hypergeometric distribution test, which calculates the probability of overlap between the up/downregulated gene set and each GO category compared against another gene list that is randomly sampled. We applied the test to the identified up/downregulated genes to test whether they are significantly enriched (false discovery rate ≤ 0.05) in each category of "biologic processes" (857 categories) as defined by the Gene Ontology database.

Results

EHMT2 *Expression Is Upregulated in Clinical Cancer Tissues*

To identify the histone methyltransferase involved in human carcinogenesis, we examined the expression profile for several histone methyltransferase genes using six clinical bladder samples, and we found a significant difference of *EHMT2* gene expression between cancer and normal tissues (data not shown). Consequently, we analyzed 118 bladder cancer samples and 26 normal control samples (British) and found a significant elevation of *EHMT2* expression in tumor cells compared with that in normal cells ($P < .0001$, Mann-Whitney *U* test) (Figure 1*A* and Table W1). No statistical significance was observed in the expression levels among cancer samples of different stages and grades (Figure 1*B*). This suggests that *EHMT2* expression was upregulated at an early stage in bladder carcinogenesis and remained high in the advanced stages of the disease. Subclassification of tumors according to metastasis status, sex, smoking history, and recurrence status identified no significant differences of *EHMT2* expression levels (data not shown). We then analyzed the expression patterns of *EHMT2* in 34 Japanese clinical bladder cancer samples by cDNA microarray (Figure 1*C* and Table 1) and confirmed a significant overexpression in bladder cancers of Japanese patients ($P < .0001$, Mann-Whitney *U* test). Consistent with this, expression levels of *EHMT2* in 12 bladder cancer cell lines were significantly higher than those in 2 normal human fibroblast cell lines (Figure W1). To evaluate protein expression levels of EHMT2 in clinical tissues, we performed immunohistochemical analysis using an anti-EHMT2 specific antibody. This antibody strongly stained the nucleus of various types of bladder cancer tissues, whereas signals in the normal bladder tissue were weak (Figure 1*D*).

In addition to bladder tissues, we examined expression levels of EHMT2 in lung tissues. cDNA microarray experiments showed that the *EHMT2* expression was highly elevated in lung tumor tissues compared with corresponding nonneoplastic tissues (Figure 2*A* and Table 1), and the overexpression of *EHMT2* in lung cancer was also validated by quantitative real-time PCR (Figure 2*B*). In addition, expression levels of *EHMT2* in four lung cancer cell lines were significantly higher than in two normal human fibroblast cell lines (Figure 2*C*). We then examined EHMT2 protein expression levels in lung tissue by immunohistochemistry (Figure 2*D*) and observed strong EHMT2 staining in the nucleus of cancer tissues and weak staining in nonneoplastic tissues. Besides, we examined the microarray expression analysis of a large number of clinical samples derived from Japanese subjects and found that *EHMT2* expression was also significantly upregulated in various types of cancer compared with corresponding nonneoplastic tissues (Table 1). These data indicate that EHMT2 may be involved in many types of human cancer.

Growth Regulation of Cancer Cells by EHMT2

To investigate the role of EHMT2 in human carcinogenesis, we performed knockdown experiments using siRNAs against EHMT2 (siEHMT2 #1 and #2) and two control siRNAs (siEGFP and siNC) (Table W2). We transfected these two independent EHMT2 siRNAs into A549 and SBC5 cells, in which EHMT2 was highly expressed (Figure 3*A*). EHMT2 expression in the transfected cells was significantly suppressed at the mRNA level, in comparison with cells transfected with control siRNAs at the mRNA level (Figure 3*B*). Using the siRNAs, we performed the cell growth assay. We observed a significant growth suppression of two bladder cancer cell lines (SW780 and RT4) and three lung cancer cell lines (LC319, A549, and SBC5) after treatment with two EHMT2 siRNAs, although no effect was observed for control siRNAs (Figure 3*C*). To further assess the mechanism of growth suppression induced by the siRNA, we analyzed the cell cycle status of cancer cells after treatment with siRNAs using flow cytometry stained with propidium iodide. The proportion of cancer cells in the G_1, S, and G_2/M phases slightly decreased and that in the sub-G_1 phase increased in a significant manner after treatment with two different EHMT2 siRNAs (Figure 3*D*). These results suggest that EHMT2 plays a crucial role in cell cycle regulation of cancer cells and that apoptosis is induced after EHMT2 knockdown.

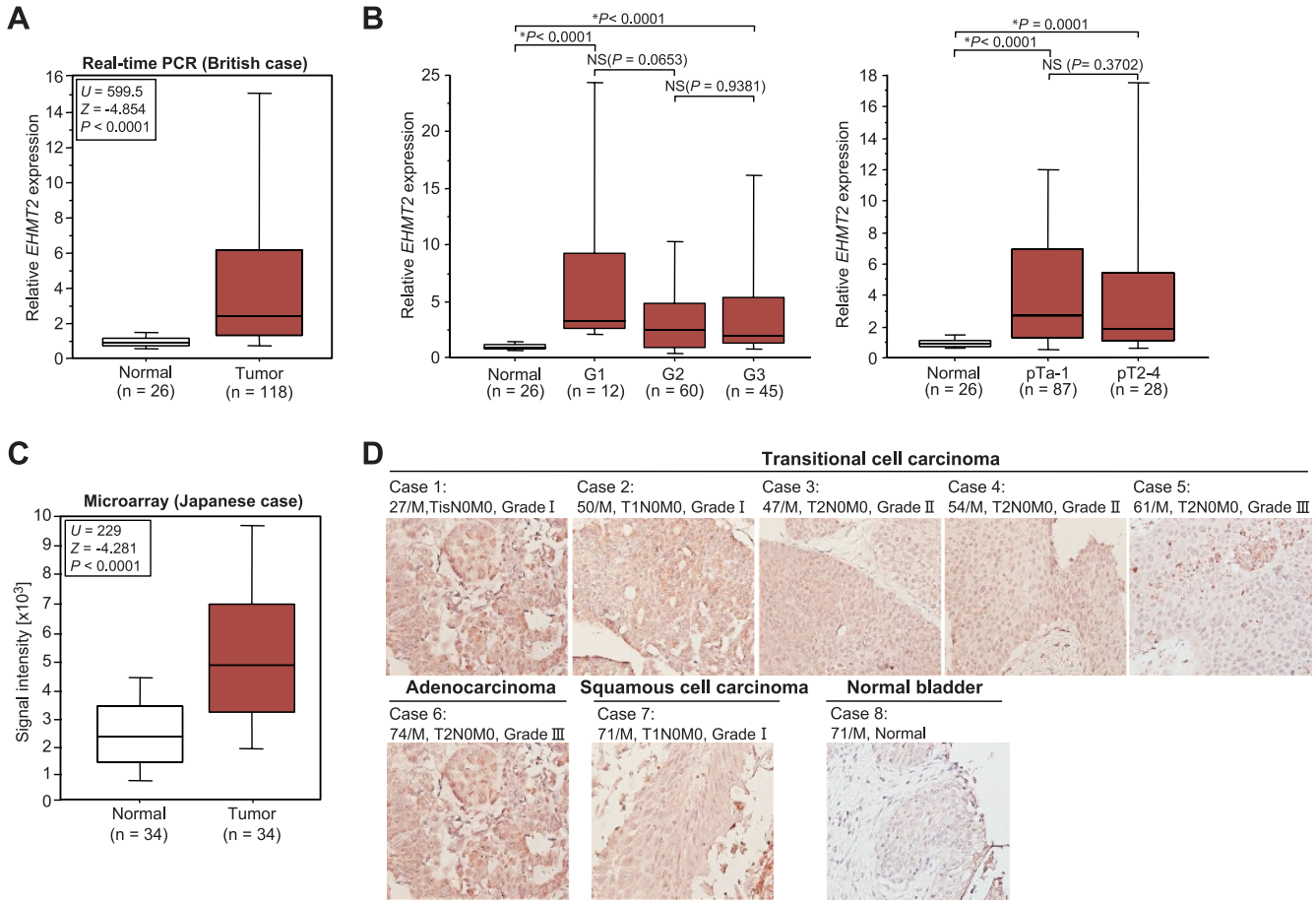

Figure 1. Elevated EHMT2 expression in bladder cancer. (A) *EHMT2* gene expression in normal and tumor bladder tissues in British cases. Expression levels of *EHMT2* were analyzed by quantitative real-time PCR, and the result is shown by box-whisker plot. Mann-Whitney *U* test was used for statistical analysis. (B) Statistical analysis of *EHMT2* expression categorized by the histologic grade (left) and pathologic stage (right) of bladder tumors. Expression levels of *EHMT2* were analyzed by quantitative real-time PCR, and the result is shown by box-whisker plot. Mann-Whitney *U* test was used for statistical analysis. NS indicates not significant. (C) Comparison of *EHMT2* expression between normal and tumor tissues in bladder cancer. Signal intensity of each sample was analyzed by cDNA microarray, and the result is shown by box-whisker plot (median, 50% boxed). Mann-Whitney *U* test was used for the statistical analysis. (D) Tissue microarray images of bladder tumors stained by standard immunohistochemistry for protein expression of EHMT2. Clinical information for each section is represented above the histologic pictures. Original magnification, ×200.

SIAH1 Directly Regulated by EHMT2 Is a Key Regulator of Cancer Cell Growth and Apoptosis

To define the mechanism by which EHMT2 regulates the cell cycle and apoptosis, we identified target genes regulated by EHMT2 using microarray expression analysis. To clarify early responding genes after knockdown of EHMT2, we isolated total RNA from SW780 and A549 cells 24 hours after treatment with siEHMT2. The expression profile of these cells was analyzed by Affymetrix's HG-U133 Plus 2.0 Array in comparison with those treated with control siRNAs (siEGFP and siFFLuc), and we identified a set of genes that were significantly up/downregulated. The sub-G_1 population of cancer cells was significantly increased by knockdown of EHMT2, according to FACS analysis (Figure 3*D*), so we hypothesized that EHMT2 could be associated with the regulation of apoptosis in cancer cells. We identified a downstream gene for EHMT2, which was known to be involved in apoptotic regulation in cancer cells, by microarray analysis. The expression of our candidate, *SIAH1*, could indeed be regulated by EHMT2 (Figure 4, *A* and *B*, *left*). Up-regulation of SIAH1 after treatment with siEHMT2 was confirmed by both quantitative real-time PCR and Western blot (Figure 4*B*, *right*, and *C*). To test whether EHMT2 transcriptionally regulates the SIAH1 expression, we performed a ChIP assay. EHMT2 protein was highly enriched at the promoter region of *SIAH1* after transfection with a 3×FLAG-EHMT2 vector together with increased

Table 1. Expression of *EHMT2* in Cancer Tissues Analyzed by cDNA Microarray*.

Tissue Type	Case (*n*)	Ratio (Tumor/Normal)		
		Count > 2	Count > 3	Count > 5
Acute myelogenous leukemia	55	26 (47.3%)	8 (14.5%)	1 (1.8%)
Bladder cancer	34	19 (55.9%)	11 (32.4%)	4 (11.8%)
Breast cancer	78	14 (17.9%)	4 (5.1%)	3 (3.8%)
Cervical Cancer	19	5 (26.3%)	1 (5.3%)	0 (0%)
Chronic myelogenous leukemia	77	46 (59.7%)	40 (51.9%)	19 (24.7%)
Esophageal cancer (SqCC)	64	23 (35.9%)	15 (23.4%)	7 (10.9%)
Non–small cell lung cancer	35	17 (48.6%)	11 (31.4%)	3 (8.6%)
Osteosarcoma	27	9 (33.3%)	4 (14.8%)	3 (11.1%)
Small cell lung cancer	15	11 (73.3%)	3 (20%)	1 (6.7%)

*We compared the signal intensity *EHMT2* between tumor tissues and corresponding nonneoplastic tissues derived from the same patient.

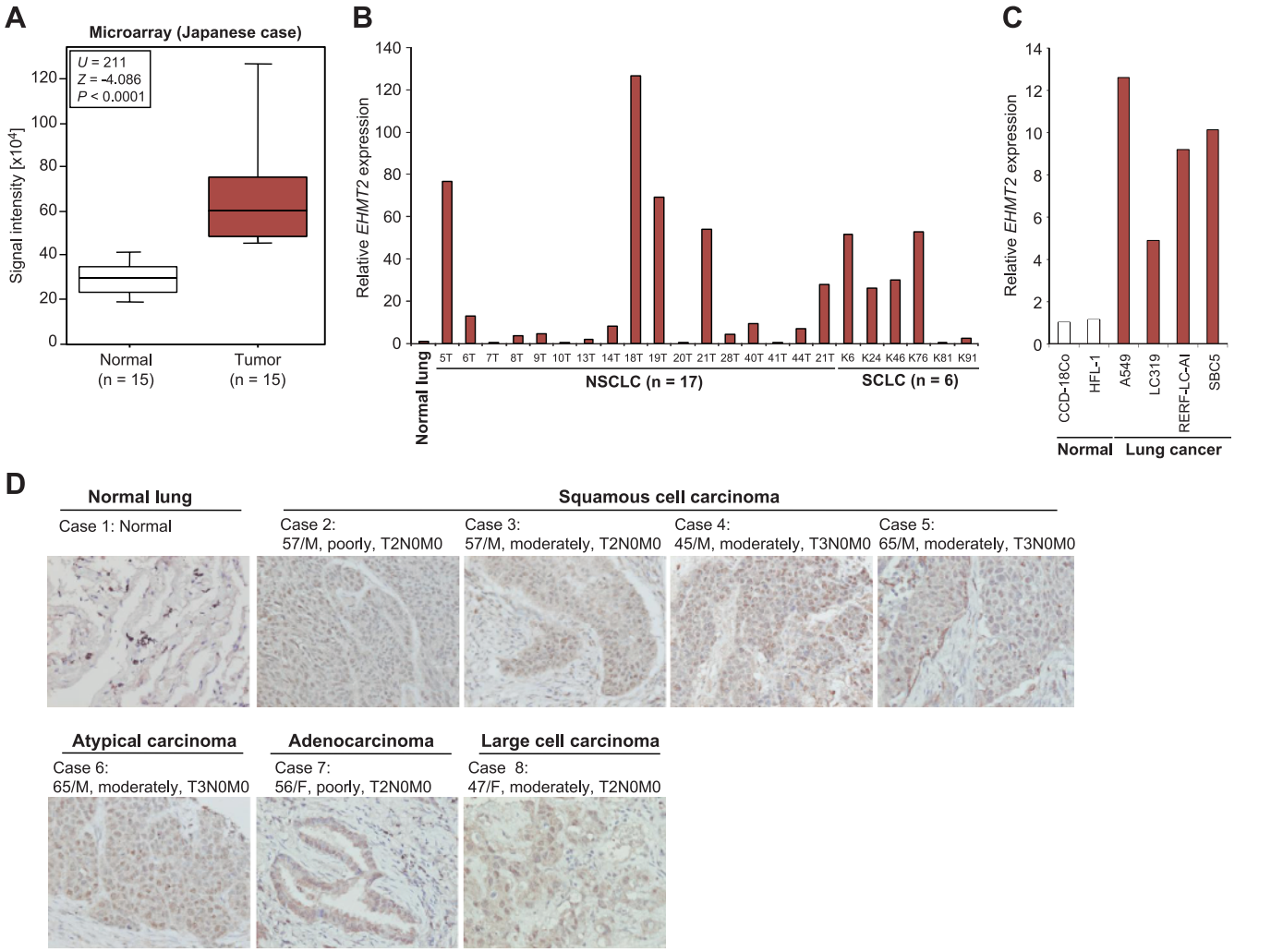

Figure 2. Elevated EHMT2 expression in lung cancer. (A) Comparison of *EHMT2* expression between normal lung and small cell lung cancer (SCLC) tissues. Signal intensity of each sample was analyzed by cDNA microarray, and the result is shown by box-whisker plot (median, 50% boxed). Mann-Whitney *U* test was used for the statistical analysis. (B) Expression of *EHMT2* in normal lung, 17 non–small cell lung cancer (NSCLC) and 6 SCLC tissues. Expression levels were analyzed by quantitative real-time PCR. Data were normalized by normal lung expressions. (C) mRNA expression levels of *EHMT2* in two normal human cell lines and four lung cancer cell lines examined by quantitative real-time PCR. Expression levels were normalized by *GAPDH* and *SDH* expressions, and values are relative to CCD-18Co (CCD-18Co = 1). (D) Immunohistochemical staining of EHMT2 in lung tissues. Clinical information for each section is represented above histologic pictures. Original magnification, ×200.

levels of dimethylation on histone H3-K9 (Figure 4*D*). In addition, to validate the function of endogenous EHMT2 protein in cancer cells, we performed ChIP analysis of cells after treatment with EHMT2 siRNA, using anti-EHMT2 and -H3K9me2 antibodies. These data showed that the siRNA treatment clearly diminished the binding of endogenous EHMT2 to the promoter region of *SIAH1* and reduced H3K9 dimethylation in the region (Figure 4*E*). Therefore, endogenous EHMT2 protein can bind to the promoter region of *SIAH1* and, through dimethylation of histone H3-K9, affect the regulation of gene expression.

We then tried to clarify the significance of SIAH1 suppressed by EHMT2 in cancer cells. Because knockdown of EHMT2 significantly increased the sub-G_1 population of cancer cells, we performed detailed apoptotic analysis using the SIAH1 siRNA whose effects were already validated. Cleaved PARP1 and caspase 3 were observed in SBC5 cells after treatment with siEHMT2, implying that apoptosis is likely to be induced by the knockdown of EHMT2. Subsequently, we examined the effects of SIAH1 knockdown on EHMT2 siRNA-induced apoptosis. Importantly, the cleavage of PARP1 and caspase 3 was not observed in SBC5 cells treated with both EHMT2 and SIAH1 siRNAs (Figure 5*A*). These data reveal that SIAH1 is an essential factor for EHMT2 siRNA-induced apoptosis. Furthermore, we conducted the growth assay after treatment with siEHMT2 and either siEGFP or siSIAH1. The growth of SBC5 cells was significantly suppressed by treatment with siEHMT2, but the growth suppression was recovered by knockdown of SIAH1 (Figure 5*B*). This result was confirmed by a colony formation assay (Figure 5*C*). Taken together, our findings suggest that SIAH1 is directly regulated by EHMT2, and it seems to play a key role in regulating growth and apoptosis of cancer cells overexpressing EHMT2.

BIX-01294 Reduced the Growth Rate of Five Cancer Cell Lines

A small molecule compound, BIX-01294 (a diazepin-quinazolin-amine derivative), specifically inhibits EHMT2 enzymatic activity and

reduces H3K9me2 levels at the chromatin regions of several EHMT2 target genes [28,29]. Because EHMT2 may be involved in the proliferation of cancer cells, we evaluated the effects of BIX-01294 on the growth of cancer cell lines. To examine the relationship between *EHMT2* expression and BIX-01294 effects, we chose cancer cells that showed a wide variety of *EHMT2* expression levels (Figure W2*A*). As shown in Figure W2*B*, the growth of cancer cells was significantly suppressed by BIX-01294 treatment in a dose-dependent manner, and the effect was correlated with *EHMT2* expression levels. The cell cycle status of SBC5 cells after treatment with BIX-01294 was examined, and the proportion of cells in the S phase significantly decreased and that in the sub-G_1 phase increased in a dose-dependent manner (Figure W2*C*). These results indicate that the enzymatic activity of EHMT2 can be closely related to the growth of cancer cells and that inhibition of EHMT2 may induce growth suppression and apoptosis of cancer cells.

Discussion

Histone modifications, including methylation, acetylation, phosphorylation, and ubiquitination, are considered to play critical roles in transcriptional activation and repression through the regulation of chromatin structure. Histone methylation was once thought to be a stable modification, but recently, it is recognized as being dynamically regulated by both histone methyltransferases and demethylases.

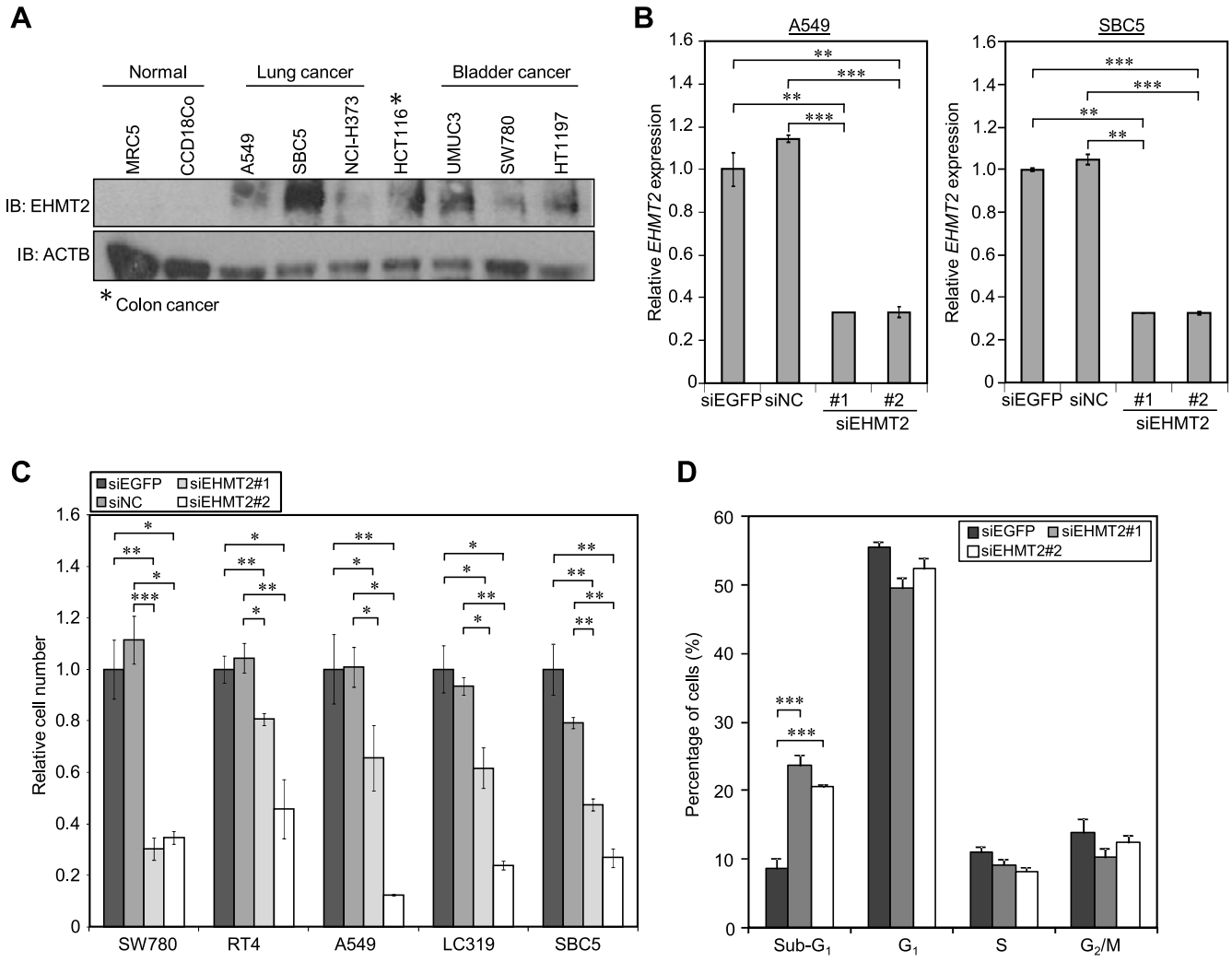

Figure 3. Involvement of EHMT2 in the growth of bladder and lung cancer cells. (A) Expression levels of EHMT2 in various cell lines. Western blot was performed to measure the protein level of EHMT2, and anti-ACTB antibody was used as an internal control. (B) Quantitative real-time PCR analysis showing suppression of endogenous expression of *EHMT2* by EHMT2-specific siRNAs (siEHMT2 #1 and #2) in A549 and SBC5 cells. siEGFP and siNC were used as controls. Relative mRNA expression shows the value normalized by expression levels of siEGFP-treated cells. Mean ± SD of three independent experiments. *P* values were calculated using Student's *t* test (***P* < .01; ****P* < .001). (C) Effects of EHMT2 siRNAs knockdown on the viability of bladder cancer cell line (SW780, RT4) and lung cancer cell lines (LC319, SBC5, A549). The relative cell number shows the value normalized to siEGFP-treated cells. Mean ± SD of three independent experiments. *P* values were calculated using Student's *t* test (**P* < .05; ***P* < .01; ****P* < .001). (D) SW780 cells were treated with siRNAs and analyzed by FACS 72 hours after siRNA treatment. We show representative histograms of this experiment. Numerical analysis of the FACS result, classifying cells by cell cycle status. The proportion of cancer cells in sub-G_1 phase is significantly higher after treatment with siEHMT2 #1 and #2 compared with control siRNAs-treated cancer cells. Mean ± SD of three independent experiments. *P* values were calculated using Student's *t* test.

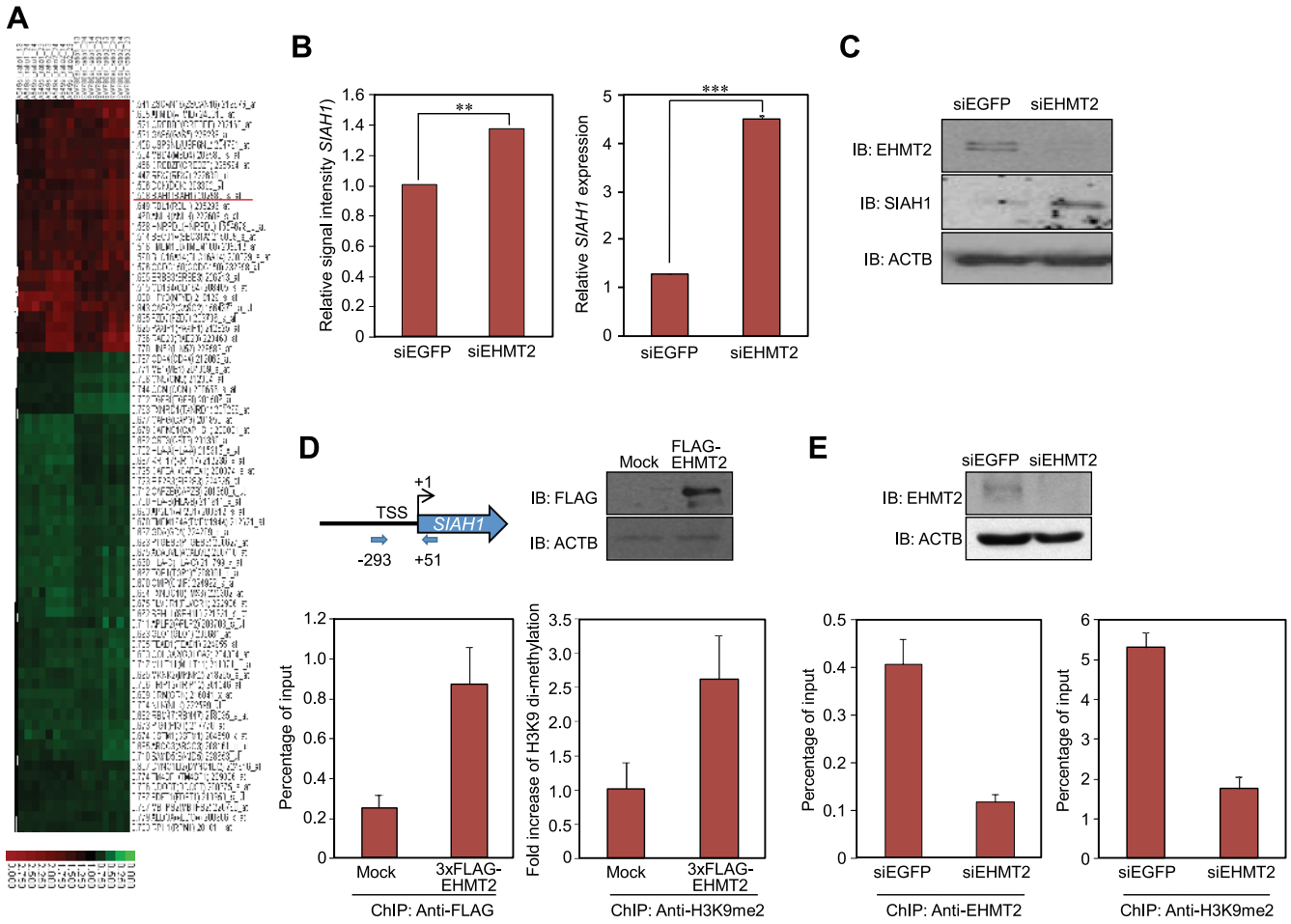

Figure 4. SIAH1 expression was directly regulated by EHMT2. (A) Two-dimensional, unsupervised hierarchical cluster analysis of SW780 and A549 cells after knockdown of *EHMT2* expression. Differentially expressed genes were selected for this analysis. Red indicates up-regulated; green, downregulated. (B) Graph of microarray result (left) and validation of microarray data using quantitative real-time PCR (right) in A549 cells after treatment with siRNAs targeting *EGFP* (control; siEGFP) and *EHMT2* (siEHMT2 #2). *P* values were calculated using Student's *t* test (**$P < .01$; ***$P < .001$). (C) Western blot analyses in A549 cells after treatment with siRNAs targeting *EGFP* (control; siEGFP) and *EHMT2* (siEHMT2 #2). Samples were fractionated by SDS-PAGE and immunoblotted with anti-EHMT2 (NB100-40825; Novus Biologicals) and -SIAH1 (sc-5506; Santa Cruz, Santa Cruz, CA) antibodies. Anti-ACTB was used as an internal control. (D) The ChIP assay was performed using anti-FLAG and -H3K9me2 antibodies after transfection with pCAGGSn-3FC (Mock) and pCAGGSn-3FC-EHMT2 (3×FLAG-EHMT2) into 293T cells. Top left: Schematic diagram of the *SIAH1* promoter region. The PCR amplified fragment is positioned by nucleotide number relatives to TSS (arrows). Bottom left: Real-time PCR analysis using a primer pair as described under Materials and Methods. Cross-linked and sheared chromatin was immunoprecipitated with anti-FLAG antibody (M2; Sigma). The result is shown as a percentage of the input chromatin. Top right: Input samples were fractionated by SDS-PAGE and immunoblotted with anti-FLAG antibody. Expression of ACTB was the internal control. Bottom right: Quantification of H3K9me2 ChIP at the *SIAH1* promoter region using real-time PCR. Cross-linked and sheared chromatin was immunoprecipitated with anti-H3K9me2 antibody (ab1220; Abcam, Cambridge, MA). (E) The ChIP assay was performed using anti-EHMT2 (bottom left) and -H3K9me2 (bottom right) antibodies after treatment of SBC5 cells with siEGFP or siEHMT2 #2 for 48 hours. The result is shown as a percentage of the input chromatin. Top: Input samples were fractionated by SDS-PAGE and immunoblotted with anti-EHMT2 antibody. Expression of ACTB was the internal control.

EHMT2 is mainly responsible for monomethylation and dimethylation of H3K9 in euchromatin, and these play a unique role in transcriptional regulation and chromatin remodeling [11–13,30,31]. In this study, we demonstrated the significant up-regulation of EHMT2 in bladder and lung cancers by quantitative RT-PCR and immunohistochemistry at the RNA and protein levels. Together with microarray-based expression profiles of a large number of clinical tissues, EHMT2 expression is considered to be dysregulated in nine human tumors (Table 1). We postulated that EHMT2 may serve an important role in the growth regulation of cancer cells and confirmed that knockdown of EHMT2 suppresses the growth of various bladder and lung cancer cells, with the number of cells in the sub-G_1 phase increasing (Figure 3, *C* and *D*). The pathway analysis using the cells in which EHMT2 expression was knocked down by siRNA indicated that EHMT2 could be involved in the regulation of cell apoptosis and a variety of chromatin functions such as chromatin remodeling and transcriptional regulation (Table W3).

It has been suggested that *SIAH1* is a tumor suppressor gene located in chromosomal band 16q12-q13, a frequently deleted region in human tumors arising from various tissues [32,33]. It was also reported that E3 ubiquitin ligases, including SIAH1, played an important role in regulating breast carcinogenesis [34], and a recent study indicated that SIAH1

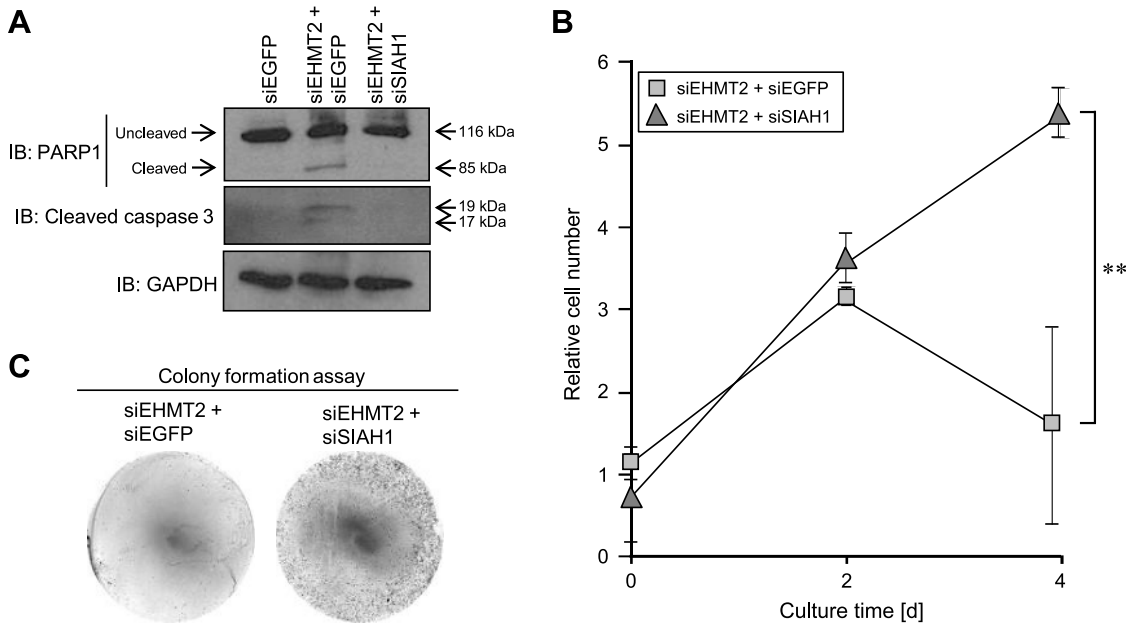

Figure 5. SIAH1 regulated by EHMT2 is a key regulator of cancer cell growth and apoptosis. (A) Western blot analyses in SBC5 cells after treatment with siRNAs targeting *EGFP* (control; siEGFP), *EHMT2* (siEHMT2 #2), and *SIAH1* (siSIAH1) for 72 hours. Anti-PARP1 (sc-8007; Santa Cruz) and –cleaved caspase 3 (no. 9661S; Cell Signaling, Danvers, MA) antibodies were used as apoptosis markers, and anti-GAPDH antibody was used as an internal control. (B) Cell growth assay of SBC5 cells treated with indicated siRNAs. siEHMT2 #2 and either siEGFP or siSIAH1 were transfected 24 hours after preparation of cells, and subsequently, cell viability was measured 48 and 96 hours after siRNA treatment. Mean ± SD of three independent experiments. *P* values were calculated using Student's *t* test (**$P < .01$). (C) Colony formation assay of SBC5 cells. Indicated siRNAs were transfected 24 hours after preparation of cells, and Giemsa staining was performed 96 hours after treatment with siRNAs.

induces apoptosis by activating the JNK pathway and inhibits invasion by inactivating the ERK pathway in breast cancer cells [22]. We previously reported that the paternally expressed gene 10 (*PEG10*), which was highly expressed in hepatocellular carcinomas, associated with SIAH1 and PEG10 overexpression decreased the cell death mediated by SIAH1 [20]. Moreover, our expression profile data show that the expression levels of SIAH1 in tumor tissues are significantly low compared with the corresponding nonneoplastic tissues in various types of cancer, including bladder and lung cancers (Table W4). These data reveal that SIAH1 is one of the key regulators in human carcinogenesis. Our microarray data showed that *SIAH1* was upregulated by EHMT2 knockdown, and we confirmed this elevation using quantitative real-time PCR and Western blot analyses. In addition, we found that EHMT2 directly binds to the promoter region of *SIAH1* and regulates the transcription of *SIAH1* through the histone methylation analyzed by ChIP assay (Figure 4, *D* and *E*). Consistently, the apoptosis induction and growth suppression after treatment with EHMT2 siRNA was recovered by SIAH1 knockdown (Figure 5). According to our series of experiments, EHMT2 directly regulates SIAH1 expression through methylation of histone H3-K9, and it may be an important mechanism on how overexpressed EHMT2 contributes to human carcinogenesis.

In the present study, we found that EHMT2 was overexpressed in various types of cancer, including bladder and lung cancers, and plays a crucial role in the proliferation of cancer cells. Importantly, the BioGPS database revealed that the expression of EHMT2 in many types of normal tissues is very low (Figure W3), indicating that EHMT2 can be an ideal target for cancer therapy. Indeed, we evaluated the effects of treatment with BIX-01294, a specific inhibitor of EHMT2, and found that this chemical compound effectively suppressed the growth of cancer cells (Figure W2). This result suggests the possibility that EHMT2 inhibitors may work as anticancer drugs. Intriguingly, it was previously reported that down-regulation of EHMT2 disrupted centrosome and chromosome stability in cancer cells, and cancer cell growth was significantly inhibited [30]. The data are consistent with our series of experiments, and inhibition of EHMT2 functions seems to be an effective tool for cancer therapy. Meanwhile, information about specificity and toxicity of BIX-01294 is largely insufficient. Further validation with functional analyses of this protein in the context of human carcinogenesis and optimization of EHMT2 inhibitors as anticancer drugs may assist to development of novel therapeutic strategies for human cancer.

Acknowledgments

The authors thank Gillian Murphy and the members of her laboratory for substantial technical support. The authors also thank Motoko Unoki for helpful discussion and Noriko Ikawa, Kazuhiro Maejima, Kazuyuki Hayashi, Yuka Yamane, Yukiko Iwai, Miyuki Saito, and Haruka Sawada for technical assistance.

References

[1] Kouzarides T (2002). Histone methylation in transcriptional control. *Curr Opin Genet Dev* **12**, 198–209.

[2] Bannister AJ, Zegerman P, Partridge JF, Miska EA, Thomas JO, Allshire RC, and Kouzarides T (2001). Selective recognition of methylated lysine 9 on histone H3 by the HP1 chromo domain. *Nature* **410**, 120–124.

[3] Lachner M, O'Carroll D, Rea S, Mechtler K, and Jenuwein T (2001). Methylation of histone H3 lysine 9 creates a binding site for HP1 proteins. *Nature* **410**, 116–120.

[4] Fischle W, Tseng BS, Dormann HL, Ueberheide BM, Garcia BA, Shabanowitz J, Hunt DF, Funabiki H, and Allis CD (2005). Regulation of HP1-chromatin binding by histone H3 methylation and phosphorylation. *Nature* **438**, 1116–1122.

[5] Hirota T, Lipp JJ, Toh BH, and Peters JM (2005). Histone H3 serine 10 phosphorylation by Aurora B causes HP1 dissociation from heterochromatin. *Nature* **438**, 1176–1180.

[6] Strahl BD and Allis CD (2000). The language of covalent histone modifications. *Nature* **403**, 41–45.

[7] Hamamoto R, Furukawa Y, Morita M, Iimura Y, Silva FP, Li M, Yagyu R, and Nakamura Y (2004). SMYD3 encodes a histone methyltransferase involved in the proliferation of cancer cells. *Nat Cell Biol* **6**, 731–740.

[8] Hamamoto R, Silva FP, Tsuge M, Nishidate T, Katagiri T, Nakamura Y, and Furukawa Y (2006). Enhanced SMYD3 expression is essential for the growth of breast cancer cells. *Cancer Sci* **97**, 113–118.

[9] Albert M and Helin K (2010). Histone methyltransferases in cancer. *Semin Cell Dev Biol* **21**, 209–220.

[10] Krivtsov AV and Armstrong SA (2007). MLL translocations, histone modifications and leukaemia stem-cell development. *Nat Rev Cancer* **7**, 823–833.

[11] Tachibana M, Sugimoto K, Fukushima T, and Shinkai Y (2001). Set domain-containing protein, G9a, is a novel lysine-preferring mammalian histone methyltransferase with hyperactivity and specific selectivity to lysines 9 and 27 of histone H3. *J Biol Chem* **276**, 25309–25317.

[12] Tachibana M, Sugimoto K, Nozaki M, Ueda J, Ohta T, Ohki M, Fukuda M, Takeda N, Niida H, Kato H, et al. (2002). G9a histone methyltransferase plays a dominant role in euchromatic histone H3 lysine 9 methylation and is essential for early embryogenesis. *Genes Dev* **16**, 1779–1791.

[13] Gyory I, Wu J, Fejer G, Seto E, and Wright KL (2004). PRDI-BF1 recruits the histone H3 methyltransferase G9a in transcriptional silencing. *Nat Immunol* **5**, 299–308.

[14] Nishio H and Walsh MJ (2004). CCAAT displacement protein/cut homolog recruits G9a histone lysine methyltransferase to repress transcription. *Proc Natl Acad Sci USA* **101**, 11257–11262.

[15] Roopra A, Qazi R, Schoenike B, Daley TJ, and Morrison JF (2004). Localized domains of G9a-mediated histone methylation are required for silencing of neuronal genes. *Mol Cell* **14**, 727–738.

[16] Lee DY, Northrop JP, Kuo MH, and Stallcup MR (2006). Histone H3 lysine 9 methyltransferase G9a is a transcriptional coactivator for nuclear receptors. *J Biol Chem* **281**, 8476–8485.

[17] Esteve PO, Chin HG, Smallwood A, Feehery GR, Gangisetty O, Karpf AR, Carey MF, and Pradhan S (2006). Direct interaction between DNMT1 and G9a coordinates DNA and histone methylation during replication. *Genes Dev* **20**, 3089–3103.

[18] Carthew RW and Rubin GM (1990). *Seven in absentia*, a gene required for specification of R7 cell fate in the *Drosophila* eye. *Cell* **63**, 561–577.

[19] Hu G, Chung YL, Glover T, Valentine V, Look AT, and Fearon ER (1997). Characterization of human homologs of the *Drosophila* seven in absentia (*sina*) gene. *Genomics* **46**, 103–111.

[20] Okabe H, Satoh S, Furukawa Y, Kato T, Hasegawa S, Nakajima Y, Yamaoka Y, and Nakamura Y (2003). Involvement of *PEG10* in human hepatocellular carcinogenesis through interaction with *SIAH1*. *Cancer Res* **63**, 3043–3048.

[21] Wen YY, Yang ZQ, Song M, Li BL, Yao XH, Chen XL, Zhao J, Lu YY, Zhu JJ, and Wang EH (2010). The expression of SIAH1 is downregulated and associated with Bim and apoptosis in human breast cancer tissues and cells. *Mol Carcinog* **49**, 440–449.

[22] Wen YY, Yang ZQ, Song M, Li BL, Zhu JJ, and Wang EH (2010). SIAH1 induced apoptosis by activation of the JNK pathway and inhibited invasion by inactivation of the ERK pathway in breast cancer cells. *Cancer Sci* **101**, 73–79.

[23] Cho HS, Suzuki T, Dohmae N, Hayami S, Unoki M, Yoshimatsu M, Toyokawa G, Takawa M, Chen T, Kurash JK, et al. (2011). Demethylation of RB regulator MYPT1 by histone demethylase LSD1 promotes cell cycle progression in cancer cells. *Cancer Res* **71**, 1–6.

[24] Unoki M, Kelly JD, Neal DE, Ponder BA, Nakamura Y, and Hamamoto R (2009). UHRF1 is a novel molecular marker for diagnosis and the prognosis of bladder cancer. *Br J Cancer* **101**, 98–105.

[25] Hayami S, Kelly JD, Cho HS, Yoshimatsu M, Unoki M, Tsunoda T, Field HI, Neal DE, Yamaue H, Ponder BA, et al. (2011). Overexpression of LSD1 contributes to human carcinogenesis through chromatin regulation in various cancers. *Int J Cancer* **128**, 574–586.

[26] Hayami S, Yoshimatsu M, Veerakumarasivam A, Unoki M, Iwai Y, Tsunoda T, Field HI, Kelly JD, Neal DE, Yamaue H, et al. (2010). Overexpression of the JmjC histone demethylase KDM5B in human carcinogenesis: involvement in the proliferation of cancer cells through the E2F/RB pathway. *Mol Cancer* **9**, 59.

[27] Yoshimatsu M, Toyokawa G, Hayami S, Unoki M, Tsunoda T, Field HI, Kelly JD, Neal DE, Maehara Y, Ponder BA, et al. (2011). Dysregulation of PRMT1 and PRMT6, type I arginine methyltransferases, is involved in various types of human cancers. *Int J Cancer* **128**, 562–573.

[28] Chang Y, Zhang X, Horton JR, Upadhyay AK, Spannhoff A, Liu J, Snyder JP, Bedford MT, and Cheng X (2009). Structural basis for G9a-like protein lysine methyltransferase inhibition by BIX-01294. *Nat Struct Mol Biol* **16**, 312–317.

[29] Kubicek S, O'Sullivan RJ, August EM, Hickey ER, Zhang Q, Teodoro ML, Rea S, Mechtler K, Kowalski JA, Homon CA, et al. (2007). Reversal of H3K9me2 by a small-molecule inhibitor for the G9a histone methyltransferase. *Mol Cell* **25**, 473–481.

[30] Kondo Y, Shen L, Ahmed S, Boumber Y, Sekido Y, Haddad BR, and Issa JP (2008). Downregulation of histone H3 lysine 9 methyltransferase G9a induces centrosome disruption and chromosome instability in cancer cells. *PLoS One* **3**, e2037.

[31] Yuan X, Feng W, Imhof A, Grummt I, and Zhou Y (2007). Activation of RNA polymerase I transcription by Cockayne syndrome group B protein and histone methyltransferase G9a. *Mol Cell* **27**, 585–595.

[32] Medhioub M, Vaury C, Hamelin R, and Thomas G (2000). Lack of somatic mutation in the coding sequence of *SIAH1* in tumors hemizygous for this candidate tumor suppressor gene. *Int J Cancer* **87**, 794–797.

[33] Okabe H, Ikai I, Matsuo K, Satoh S, Momoi H, Kamikawa T, Katsura N, Nishitai R, Takeyama O, Fukumoto M, et al. (2000). Comprehensive allelotype study of hepatocellular carcinoma: potential differences in pathways to hepatocellular carcinoma between hepatitis B virus–positive and –negative tumors. *Hepatology* **31**, 1073–1079.

[34] Chen C, Seth AK, and Aplin AE (2006). Genetic and expression aberrations of E3 ubiquitin ligases in human breast cancer. *Mol Cancer Res* **4**, 695–707.

Supplemental Data

Materials and Methods

Tissue samples and RNA preparation. Bladder tissue samples and RNA preparation were described previously [1]. Briefly, 126 surgical specimens of primary urothelial carcinoma were collected, either at cystectomy or at transurethral resection of bladder tumor (TUR-Bt) and snap-frozen in liquid nitrogen. A total of 26 normal bladder tissues were collected from areas of macroscopically normal regions in patients with no evidence of malignancy. Five sequential sections of 7-μm thickness were cut from each tissue and stained using Histogene staining solution (Arcturus, Oxnard, CA) following the manufacturer's protocol and assessed for cellularity and tumor grade by an independent consultant urohistopathologist. Approximately 10,000 cells were microdissected from both stromal and epithelial/tumor compartments in each tissue. To validate the accuracy of microdissection, primers and probes for Vimentin and Uroplakin were sourced and quantitative RT-PCR was performed according to the manufacturer's instructions (Assays-on-Demand; Applied Biosystems). Vimentin is primarily expressed in mesenchymally derived cells and used as a stromal marker. Uroplakin is a marker of urothelial differentiation and is preserved in up to 90% of epithelially derived tumors [2]. Use of tissues for this study was approved by Cambridge shire Local Research Ethics Committee (ref. 03/018).

Expression profiling in cancers using cDNA microarrays. We established a genome-wide cDNA microarray with 36,864 cDNAs or ESTs selected from the UniGene database of the National Center for Biotechnology Information. This microarray system was constructed essentially as described previously [3-5]. Briefly, the cDNAs were amplified by RT-PCR using poly(A)$^+$ RNAs isolated from various human organs as templates; the lengths of the amplicons ranged from 200 to 1100 bp, without any repetitive or poly(A) sequences. Many types of tumors and corresponding nonneoplastic tissues were prepared in 8-μm sections, as described previously [4]. A total of 30,000 to 40,000 cancer or noncancerous cells were collected selectively using the EZ cut system (SL Microtest GmbH, Jena, Germany) according to the manufacturer's protocol. Extraction of total RNA, T7-based amplification, and labeling of probes were performed as described previously [4]. Aliquots (2.5 μg) of twice-amplified RNA (aRNA) from each cancerous and noncancerous tissue were then labeled, respectively, with Cy3-dCTP or Cy5-dCTP. Detailed expression profiling data of bladder and lung cancers, shown in this study, were based on the data reported previously by Drs Ryo Takata and Takefumi Kikuchi, respectively [3,6].

References

[1] Wallard MJ, Pennington CJ, Veerakumarasivam A, Burtt G, Mills IG, Warren A, Leung HY, Murphy G, Edwards DR, Neal DE, et al. (2006). Comprehensive profiling and localisation of the matrix metalloproteinases in urothelial carcinoma. *Br J Cancer* **94**, 569–577.

[2] Olsburgh J, Harnden P, Weeks R, Smith B, Joyce A, Hall G, Poulsom R, Selby P, and Southgate J (2003). Uroplakin gene expression in normal human tissues and locally advanced bladder cancer. *J Pathol* **199**, 41–49.

[3] Kikuchi T, Daigo Y, Katagiri T, Tsunoda T, Okada K, Kakiuchi S, Zembutsu H, Furukawa Y, Kawamura M, Kobayashi K, et al. (2003). Expression profiles of non–small cell lung cancers on cDNA microarrays: identification of genes for prediction of lymph-node metastasis and sensitivity to anti-cancer drugs. *Oncogene* **22**, 2192–2205.

[4] Kitahara O, Furukawa Y, Tanaka T, Kihara C, Ono K, Yanagawa R, Nita ME, Takagi T, Nakamura Y, and Tsunoda T (2001). Alterations of gene expression during colorectal carcinogenesis revealed by cDNA microarrays after laser-capture microdissection of tumor tissues and normal epithelia. *Cancer Res* **61**, 3544–3549.

[5] Nakamura T, Furukawa Y, Nakagawa H, Tsunoda T, Ohigashi H, Murata K, Ishikawa O, Ohgaki K, Kashimura N, Miyamoto M, et al. (2004). Genome-wide cDNA microarray analysis of gene expression profiles in pancreatic cancers using populations of tumor cells and normal ductal epithelial cells selected for purity by laser microdissection. *Oncogene* **23**, 2385–2400.

[6] Takata R, Katagiri T, Kanehira M, Tsunoda T, Shuin T, Miki T, Namiki M, Kohri K, Matsushita Y, Fujioka T, et al. (2005). Predicting response to methotrexate, vinblastine, doxorubicin, and cisplatin neoadjuvant chemotherapy for bladder cancers through genome-wide gene expression profiling. *Clin Cancer Res* **11**, 2625–2636.

Table W1. Clinicopathologic Characteristics and *EHMT2* Expression.

Tissue	Sample Name	EHMT2	Stage	Grade
Tumor	BT2	38.154	T4	3
	BT5	7.597	Ta	
	BT6	2.488	Ta	2
	BT8	0.809	Ta	2
	BT9	0.021	Ta	2
	BT10	9.196	T2	3
	BT15	3.718	T2	3
	BT16	2.943	Ta	2
	BT18	8.825	Ta	3
	BT20	0.305	T1	2
	BT21	4.680	Ta	3
	BT22	18.100	T2	2
	BT23	7.790	T1	2
	BT27	2.243	T3	3
	BT28	22.929	Ta	1
	BT31	7.520	Ta	2
	BT32	1.898	T2	3
	BT33	2.310	T1	2
	BT34	2.800	Ta	2
	BT36	0.963	T2	3
	BT38	7.842	Ta	2
	BT39	0.302	T1	3
	BT40	1.259	T2	3
	BT41	0.633	T1	2
	BT42	0.644	T2	3
	BT43	2.295	Ta	1
	BT44	0.481	T1	2
	BT46	4.627	Ta	2
	BT48	8.698	T2	3
	BT49	5.598	Ta	1
	BT50	10.781	T1	3
	BT51	31.680	Ta	2
	BT52	2.046	T3	3
	BT53	9.685	Ta	2
	BT54	0.722	T1	3
	BT56	16.182	T2	3
	BT57	1.752	T1	2
	BT58	9.347	Ta	2
	BT59	0.662	T2	3
	BT60	3.617	Mets	3
	BT64	1.602	Ta	2
	BT66	2.831	Ta	1
	BT67	0.402	T1	2
	BT68	4.220	Ta	2
	BT69	10.400	Ta	2
	BT70	3.590	T1	2
	BT71	2.750	T1	3
	BT72	27.900	Ta	1
	BT74	12.300	Ta	1
	BT76	2.730	T1	1
	BT77	4.420	Ta	2
	BT78	1.629	T1	3
	BT79	0.921	Ta	2
	BT80	2.485	Ta	2
	BT81	2.243	Ta	2
	BT82	1.629	T1	3
	BT83	0.921	Ta	2
	BT84	27.809	Ta	2
	BT85	1.874	T1	2
	BT87	2.045	T2	2
	BT88	12.620	T1	3
	BT90	4.001	Ta	2
	BT92	3.184	T1	2
	BT93	1.557	T2	3
	BT94	3.563	Ta	1
	BT95	1.111	T3a	3
	BT96	2.485	Ta	1
	BT97	0.192	Ta	2
	BT98	2.121	Ta	2
	BT99	2.078	T1	2
	BT100	53.775	T1	3
	BT101	5.750	T2	3
	BT103	3.240	T1	2
	BT105	0.514	T2	2
	BT106	1.300	Ta	3
	BT107	1.570	Mets	3
	BT108	0.027	T1	2
	BT109	27.900	Ta	2
	BT110	0.703	T1	2
	BT112	92.800	Ta	3
	BT113	0.984	T1	3
	BT114	1.910	T2	3
	BT115	1.800	T1	3
	BT116	2.160	T2a	3
	BT119	0.788	Ta	2
	BT120	2.670	Ta	2
	BT122	1.980	T1	3
	BT125	1.970	T1	2
	BT127	9.672	T1	2
	BT128	6.160	Ta	1
	BT129	0.576	Ta	2
	BT130	7.240	Ta	2
	BT131	1.574	T2	3
	BT132	0.908	T2	3
	BT133	1.367	T1	2
	BT135	1.419	T2	3
	BT137	0.221	Ta	2
	BT138	2.925	Ta	1
	BT139	1.194	T2	3
	BT140	5.000	Ta	2
	BT141	1.310	Mets	3
	BT143	1.550	T1	3
	BT145	1.320	T2	2
	BT150	0.854	Ta	2
	BT151	0.964	Ta	3
	BT152	10.261	Ta	2
	BT154	3.450	T1	3
	BT158	10.420	Ta	2
	BT160	0.780	T1	2
	BT161	3.190	Ta	2
	BT164	1.477	Ta	1
	BT169	5.186	T2	3
	BT178	2.940	Ta	2
	BT180	0.955	T1	2
	BT181	0.749	T2	3
	BT187	2.364	Ta	2
	BT188	18.595	T2	3
	BT189	4.517	T1	2
Normal	BN11A	1.142	Normal	Normal
	BN11B	1.494	Normal	Normal
	BN12A	1.858	Normal	Normal
	BN13A	0.601	Normal	Normal
	BN13B	0.962	Normal	Normal
	BN14A	1.216	Normal	Normal
	BN14B	0.677	Normal	Normal
	BN15A	0.693	Normal	Normal
	BN17B	0.533	Normal	Normal
	BN18	3.260	Normal	Normal
	BN18B	9.540	Normal	Normal
	BN19A	0.765	Normal	Normal
	BN1A	0.863	Normal	Normal
	BN20B	0.900	Normal	Normal
	BN21A	0.955	Normal	Normal
	BN22A	1.157	Normal	Normal
	BN22B	0.876	Normal	Normal
	BN24B	0.881	Normal	Normal
	BN25A	0.765	Normal	Normal
	BN26A	1.350	Normal	Normal
	BN2A	1.840	Normal	Normal
	BN2B	1.091	Normal	Normal
	BN4A	1.151	Normal	Normal
	BN4B	0.835	Normal	Normal
	BN5B	0.610	Normal	Normal
	BN6A	1.094	Normal	Normal
	BN8A	0.891	Normal	Normal
	BN9A	0.889	Normal	Normal

Table W1. (*continued*).

Table W2. siRNA Sequence.

siRNA Name		Sequence
siEGFP		Sense: 5′ GCAGCACGACUUCUUCAAGTT 3′ Antisense: 5′ CUUGAAGAAGUCGUGCUGCTT 3′
siFFLuc		Sense: 5′ GUGCGCUGCUGGUGCCAACTT 3′ Antisense: 5′ GUUGGCACCAGCAGCGCACTT 3′
siNegative control (cocktail)	Target #1	Sense: 5′ AUCCGCGCGAUAGUACGUA 3′ Antisense: 5′ UACGUACUAUCGCGCGGAU 3′
	Target #2	Sense: 5′ UUACGCGUAGCGUAAUACG 3′ Antisense: 5′ CGUAUUACGCUACGCGUAA 3′
	Target #3	Sense: 5′ UAUUCGCGCGUAUAGCGGU 3′ Antisense: 5′ ACCGCUAUACGCGCGAAUA 3′
siEHMT2 #1		Sense: 5′ GAGUUUGGCUAUGAGGCUATT 3′ Antisense: 5′ UAGCCUCAUAGCCAAACUCTT 3′
siEHMT2 #2		Sense: 5′ GCAAAUAUUUCACCUGCCATT 3′ Antisense: 5′ UGGCAGGUGAAAUAUUUGCTT 3′
siSIAH1		Sense: 5′ CGAUUGACUUGGGAAGCGATT 3′ Antisense: 5′ UCGCUUCCCAAGUCAAUCGTT 3′

Table W3. Gene Ontology Pathway Analysis Based on the Affymetrix's Microarray Data.

Entry ID	Name	Definition	*P*
GO0003677	DNA binding	Interacting selectively with DNA (deoxyribonucleic acid).	4.7×10^{-6}
GO0045449	Regulation of transcription	Any process that modulates the frequency, rate, or extent of the synthesis of either RNA on a template of DNA or DNA on a template of RNA.	4.0×10^{-6}
GO0051726	Regulation of cell cycle	Any process that modulates the rate or extent of progression through the cell cycle.	3.0×10^{-6}
GO0006355	Regulation of transcription, DNA-dependent	Any process that modulates the frequency, rate, or extent of DNA-dependent transcription.	3.2×10^{-5}
GO0004605	Phosphatidate cytidylyltransferase activity	Catalysis of the reaction: CTP + phosphatidate = diphosphate + CDP-diacylglycerol.	9.7×10^{-4}
GO0031570	DNA integrity checkpoint	Any cell cycle checkpoint that delays or arrests cell cycle progression in response to changes in DNA structure.	8.5×10^{-4}
GO0000075	Cell cycle checkpoint	A point in the eukaryotic cell cycle where progress through the cycle can be halted until conditions are suitable for the cell to proceed to the next stage.	5.8×10^{-4}
GO0051338	Regulation of transferase activity	Any process that modulates the frequency, rate, or extent of transferase activity, the catalysis of the transfer of a group, e.g., a methyl group, glycosyl group, acyl group, phosphorus-containing, or other groups, from one compound (generally regarded as the donor) to another compound (generally regarded as the acceptor). Transferase is the systematic name for any enzyme of EC class 2.	3.6×10^{-4}
GO0016481	Negative regulation of transcription	Any process that stops, prevents, or reduces the frequency, rate, or extent of transcription.	2.2×10^{-4}
GO0000278	Mitotic cell cycle	Progression through the phases of the mitotic cell cycle, the most common eukaryotic cell cycle, which canonically comprises four successive phases called G_1, S, G_2, and M and includes replication of the genome and the subsequent segregation of chromosomes into daughter cells. In some variant cell cycles, nuclear replication or nuclear division may not be followed by cell division, or G_1 and G_2 phases may be absent.	1.6×10^{-4}
GO0016564	Transcription repressor activity	Any transcription regulator activity that prevents or downregulates transcription.	1.4×10^{-4}
GO0007346	Regulation of mitotic cell cycle	Any process that modulates the rate or extent of progress through the mitotic cell cycle.	3.6×10^{-3}
GO0045892	Negative regulation of transcription, DNA-dependent	Any process that stops, prevents, or reduces the frequency, rate, or extent of DNA-dependent transcription.	3.4×10^{-3}
GO0016568	Chromatin modification	The alteration of DNA or protein in chromatin, which may result in changing the chromatin structure.	2.5×10^{-3}
GO0008629	Induction of apoptosis by intracellular signals	Any process induced by intracellular signals that directly activates any of the steps required for cell death by apoptosis.	2.2×10^{-3}
GO0006281	DNA repair	The process of restoring DNA after damage. Genomes are subject to damage by chemical and physical agents in the environment and by free radicals or alkylating agents endogenously generated in metabolism. DNA is also damaged because of errors during its replication. A variety of different DNA repair pathways have been reported that include direct reversal, base excision repair, nucleotide excision repair, photoreactivation, bypass, double-strand break repair pathway, and mismatch repair pathway.	1.52×10^{-3}
GO0007093	Mitotic cell cycle checkpoint	A signal transduction–based surveillance mechanism that ensures accurate chromosome replication and segregation by preventing progression through a mitotic cell cycle until conditions are suitable for the cell to proceed to the next stage.	1.05×10^{-3}
GO0006350	Transcription	The synthesis of either RNA on a template of DNA or DNA on a template of RNA.	1.02×10^{-3}
GO0006917	Induction of apoptosis	A process that directly activates any of the steps required for cell death by apoptosis.	4.2×10^{-2}
GO0043065	Positive regulation of apoptosis	Any process that activates or increases the frequency, rate, or extent of cell death by apoptosis.	4.2×10^{-2}
GO0008624	Induction of apoptosis by extracellular signals	Any process that activates or increases the frequency, rate, or extent of cell death by apoptosis.	2.2×10^{-2}

Table W4. Expression of *SIAH1* in Cancer Tissues Analyzed by cDNA Microarray*.

Tissue Type	Case (*n*)	Ratio (Tumor/Normal)			
		Count < 1/2	Count < 1/3	Count < 1/5	Count < 1/10
Bladder cancer	33	19 (57.5%)	17 (51.5%)	15 (45.4%)	11 (33.3%)
Breast cancer	41	27 (65.8%)	23 (56.0%)	16 (39.0%)	9 (21.9%)
Cholangiocellular carcinoma	25	17 (68.0%)	14 (56.0%)	12 (48.0%)	11 (44.0%)
Non–small cell lung cancer	26	16 (61.5%)	14 (53.8%)	11 (42.3%)	9 (34.6%)
Prostate cancer	50	22 (44.0%)	18 (36.0%)	15 (30.0%)	4 (8.0%)
Small cell lung cancer	15	11 (73.3%)	7 (46.6%)	1 (6.6%)	0 (0.0%)

*We compared the signal intensity of *SIAH1* between tumor tissues and corresponding nonneoplastic tissues derived from the same patient.

Table W5. Primer Sequences for Quantitative RT-PCR and ChIP Analyses.

Gene Name	Primer Sequence
GAPDH (housekeeping gene)- f	5′ GCAAATTCCATGGCACCGTC 3′
GAPDH (housekeeping gene)- r	5′ TCGCCCCACTTGATTTTGG 3′
SDH (housekeeping gene)- f	5′ TGGGAACAAGAGGGCATCTG 3′
SDH (housekeeping gene)- r	5′ CCACCACTGCATCAAATTCATG 3′
EHMT2- f1	5′ GGAGGAAGCTGAACTCAGGAGG 3′
EHMT2- r1	5′ GACTGAAGTCATCACCCACCAC 3′
SIAH1- f1	5′ GTTACCGCCCATTCTTCAAT 3′
SIAH1- r1	5′ GACAACATGTGAGCTTTGGG 3′
SIAH1-ChIP- f1	5′ AGCAACGGTAGCCGAGTAG 3′
SIAH1-ChIP- r1	5′ TGGCCGCCGCCGCCGCCGTTTCGC 3′

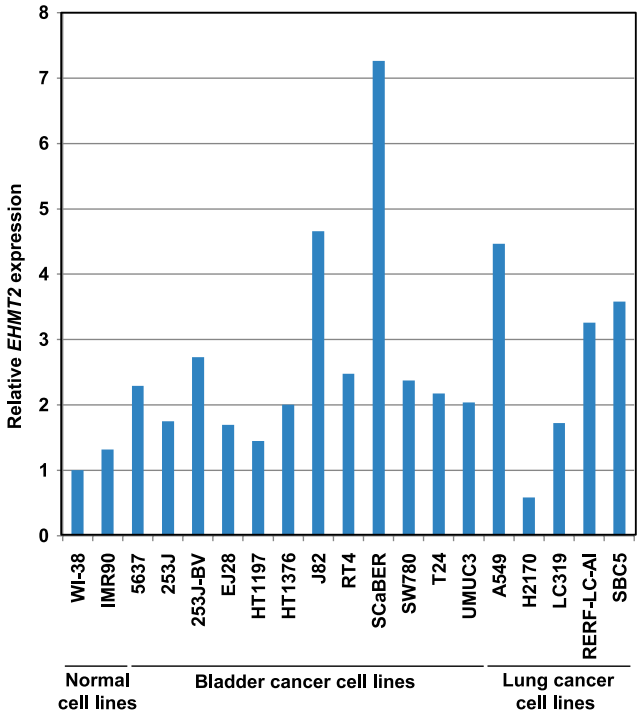

Figure W1. Expression of *EHMT2* in 2 normal cell lines, 12 bladder cancer cell lines, and 5 lung cancer cell lines. Expression levels of *EHMT2* were analyzed by quantitative real-time PCR. Data were normalized by *GAPDH* and *SDH* expressions.

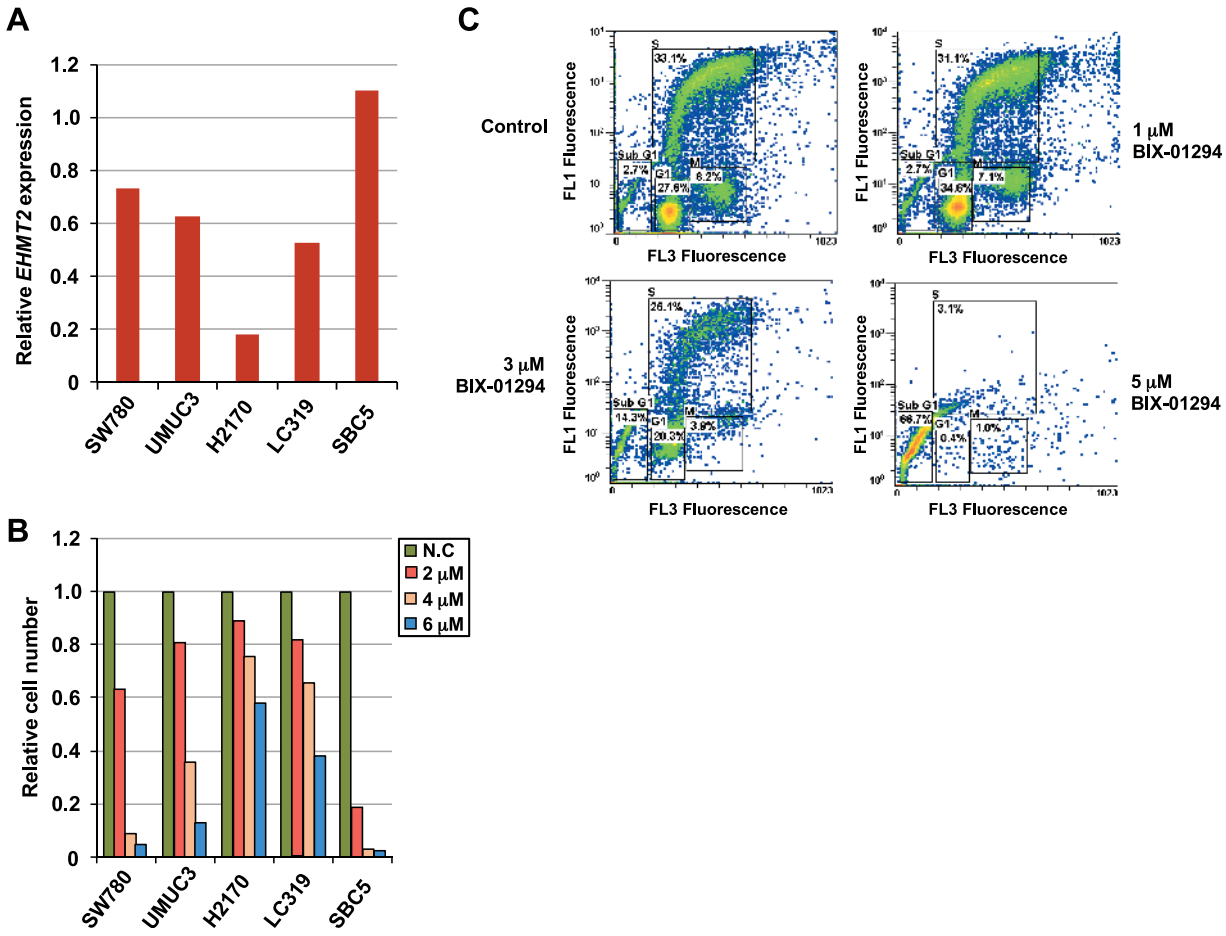

Figure W2. BIX-01294 reduces growth rate in five cancer cell lines. (A) Expression levels of *EHMT2* in five cancer cells analyzed by quantitative real-time PCR. (B) Effect of BIX-01294 on the viability of cancer cell lines. Cancer cell lines were treated for 2 days with the inhibitor BIX-01294 (2, 4, and 6 μM). This result was normalized by negative control (NC); pure water. Statistical analysis was done based on three independent experiments. *P* values were calculated using Student's *t* test. (C) Cell cycle distribution was analyzed by flow cytometry after coupled staining with fluorescein isothiocyanate (FITC)–conjugated anti-BrdU and 7-amino-actinomycin D (7-AAD) as described in Materials and Methods.

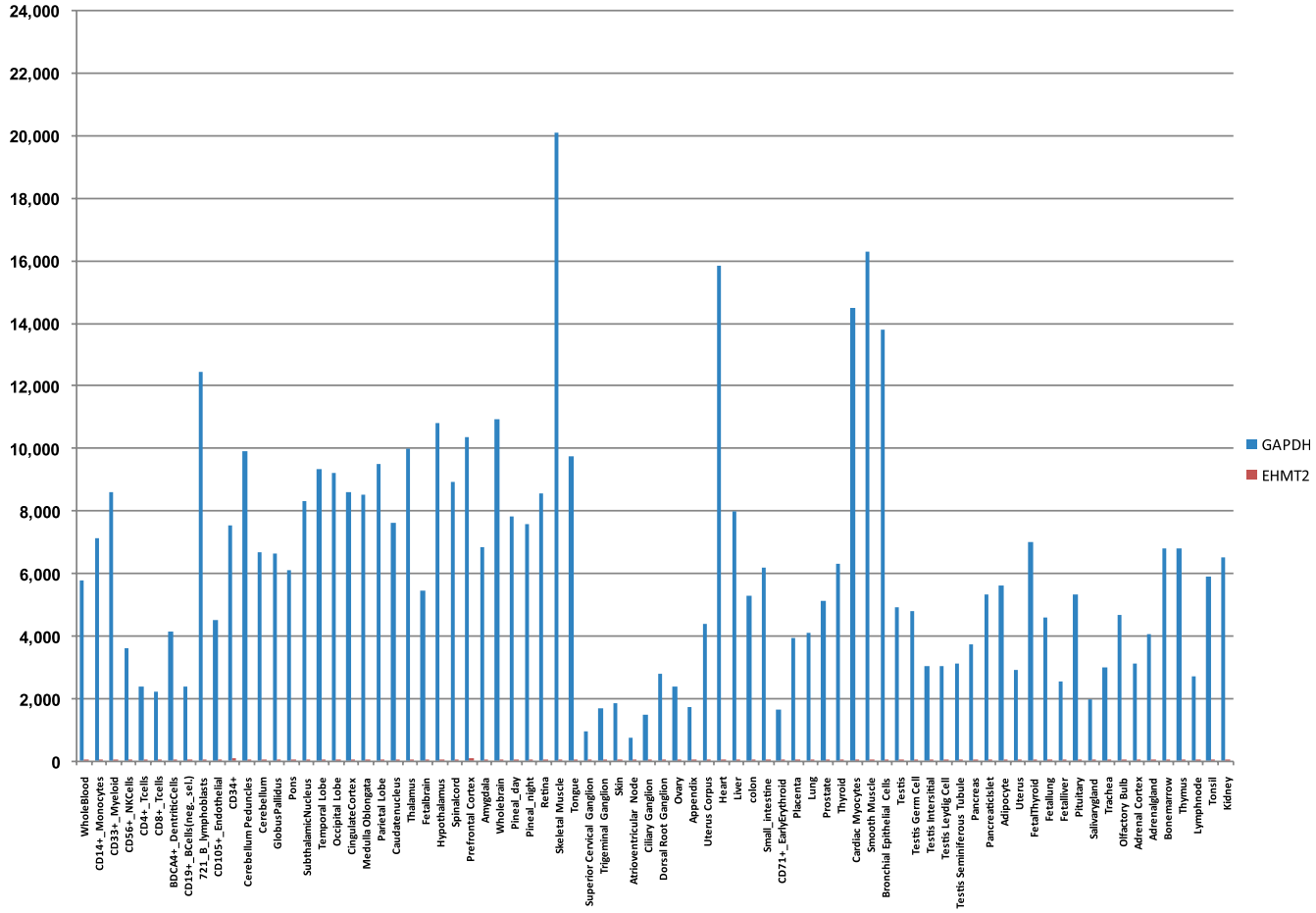

Figure W3. Expression levels of *EHMT2* in 78 normal tissues. Data were derived from BioGPS (http://biogps.gnf.org/#goto=welcome). *GAPDH* expression is shown as a control of the signal intensity.